Computational insights into the substrate recognition mechanism of cartilage extracellular matrix degradation

Yen-Yu Lai [a,1], Deng Li [a,1], Shu-Wei Chang [a,b,*]

[a] National Taiwan University, Department of Civil Engineering, Taipei 10617, Taiwan
[b] National Taiwan University, Department of Biomedical Engineering, Taipei 10617, Taiwan

A R T I C L E   I N F O

A B S T R A C T

Articular cartilage is connective tissue that forms a slippery load-bearing joint surface between bones. With outstanding mechanical properties, it plays an essential role in cushioning impact and protecting the ends of bones. Abnormal mechanical stimulation, such as repetitive overloading or chondral injury, induces excessive cartilage extracellular matrix (ECM) degradation, leading to osteoarthritis and other joint disorders. A disintegrin and metalloproteinase with thrombospondin motifs-5 (ADAMTS-5) is an aggrecanase that dominates the catalysis of aggrecan, the major proteoglycan in the cartilage ECM. Intriguingly, unlike its critical cleavage site Glu^{373}–^{374}Ala, another potential cleavage site, Glu^{419}-^{420}Ala, composed of the same amino acids in the aggrecan interglobular domain, is not a major cleavage site. It remains unclear how ADAMTS-5 distinguishes between them and hydrolyzes the correct scissile bonds. This research introduces a bottom-up in silico approach to reveal the molecular mechanism by which ADAMTS-5 recognizes the cleavage site on aggrecan. It is hypothesized that the sequence in the vicinity assists ADAMTS-5 in positioning the cleavage site. Specific residues were found to serve as binding sites, helping aggrecan bind more stably and fit into the enzyme better. The findings provide insight into the substrate binding and recognition mechanism for cartilage ECM degradation from a brand new atomic-scale perspective, laying the foundation for prophylaxis and treatment of related joint diseases.

1. Introduction

Articular cartilage is a critical structural component in the body; it lines the articulating ends of bones and provides joints with biomechanical properties [1,2]. Articular cartilage helps to dissipate mechanical loading, facilitates proper joint movement, and provides relatively low friction for joint surfaces, all of which are essential for articular movement [3,4]. Such complex mechanical properties underlie in the molecular characteristics of the cartilage extracellular matrix (ECM). The cartilage ECM is a complex system primarily composed of two constituents: the collagenous network and proteoglycans (PGs) [5]. Constituting 80%–90% of the collagenous network, type II collagen is the main component of the cartilage ECM. For PGs in cartilage, aggrecan is the dominant

form and the main determinant of cartilage's remarkable biomechanical properties (Fig. 1) [6,7].

Aggrecan mainly comprises three globular domains from its amino terminus to carboxyl terminus: G1, G2, and G3. The G1 and G2 domains are connected by the interglobular domain (IGD), and the G2 and G3 domains are connected by the glycosaminoglycan chain domain. The glycosaminoglycan chain domain is largely decorated with negatively charged chondroitin sulfate monomers and keratan sulfate monomers, which bind to several water molecules, contributing to the cartilage's excellent mechanical properties of cartilage mentioned above. In articular cartilage, numerous aggrecan molecules are linked to hyaluronan through noncovalent bonds with link proteins, forming multimolecular aggrecan aggregates (Fig. 2a) [8–10].

When the articular cartilage is injured by trauma or excessive mechanical loading, focal degradation of the cartilage and remodeling of the subchondral bone occur, resulting in joint pain and dysfunction; this condition is clinically identified as osteoarthritis (OA) [10–14]. The causes of this disease are related to abnormal ECM degradation—especially of aggrecan—in the articular cartilage

---
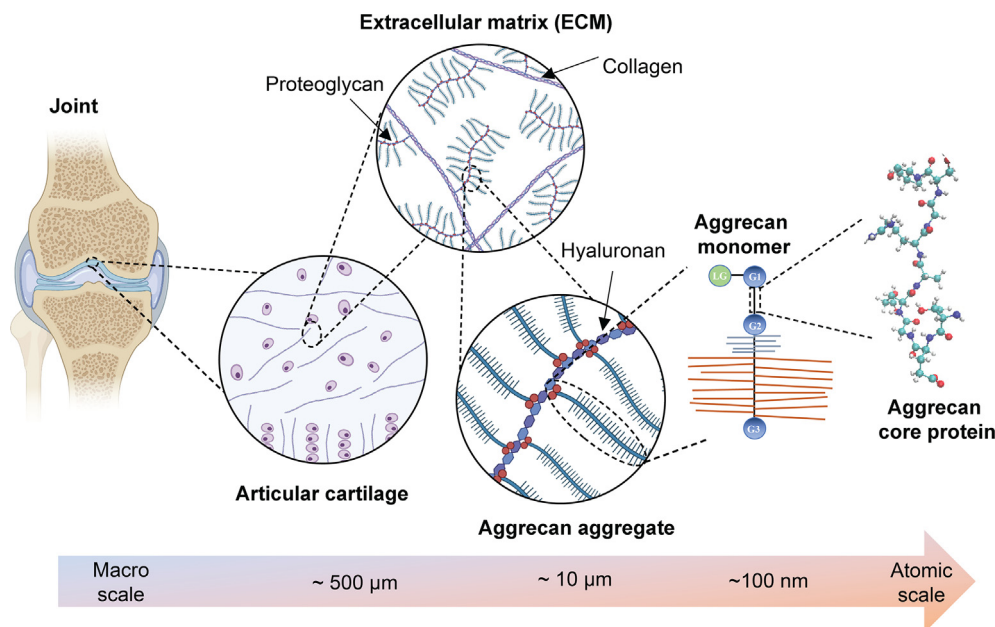
Fig. 1. The hierarchical structure of cartilage ranges from macroscale cartilage to the nanoscale aggrecan core protein. Created with BioRender.com.

[15,16]. In its normal state, aggrecan can protect collagen from degradation. Through in vitro experiments, studies have found that type II collagen can only be degraded slowly after aggrecan has been degraded. With excessive mechanical loading, the core protein of aggrecan is catalytically hydrolyzed [1,2]. After the core protein is hydrolyzed, type II collagen loses the protection of aggrecan and is further hydrolyzed by enzymes. This indicates that the degradation of aggrecan directly affects the function of articular cartilage.

Aggrecan degradation is initiated by cleavage of the core protein. The cleavage sites can be classified into two parts, which are cleaved by aggrecanases and matrix metalloproteinases (MMPs) (Fig. 2b) [17]. The IGD of the aggrecan core protein is highly sensitive to proteolysis [18]. More crucially, the site Glu^{373}–^{374}Ala in the IGD is the most critical catalytic cleavage site [10]. Aggrecan proteolysis here is extremely damaging to tissue function. Aggrecan degradation at the catalytic cleavage site Glu^{373}–^{374}Ala is mainly facilitated by a disintegrin and metalloproteinase with thrombospondin motifs-5 (ADAMTS-5) and MMP-8 [18–21]. ADAMTS-5 and MMP-8 are families of zinc metalloenzymes, which contain catalytic zinc ions at their active sites. The catalytic zinc ion participates in the catalytic mechanism of the enzyme directly, coordinating to the carbonyl group of the substrate during catalysis. Acting as an electrophilic catalyst, the zinc ion helps stabilize the developing negatively charged carbonyl oxygen of the substrate and facilitates the deprotonation of the zinc-bound water molecule, which acts as a nucleophile attacking the carbonyl carbon of the scissile bond during the hydrolysis reaction [22–25]. By analyzing the sequence in aggrecan IGD, another non-cleavage site (Glu^{419}–^{420}Ala) composed of the same amino acids was found, but only the site Glu^{373}–^{374}Ala was cleaved by enzymes. That is, scissile bond hydrolysis occurs at only the unique catalytic cleavage site despite the presence of an identical bond elsewhere (Fig. 2c). The molecular mechanism underlying the recognition of the catalytic cleavage site has not yet been revealed. Understanding the molecular mechanism by which differences in nearby sequences in the aggrecan core protein enable the catalytic cleavage site to be cleaved by the enzymes is crucial.

Bottom-up computational approaches have been successfully used to explore the molecular mechanism of ECM degradation at the nanoscale that cannot feasibly be investigated experimentally [26–28]. In this study, a bottom-up computational approach was employed to study the molecular mechanism associated with the catalytic cleavage site and non-cleavage site based on three aspects (binding conformation, binding affinity, and final binding state) for the purpose of exploring how nearby sequences enable ADAMTS-5 to recognize the catalytic cleavage site. Understanding these relationships allows us to obtain a deeper understanding of the catalytic mechanism of ADAMTS-5, facilitating the development of skeletal regenerative medicine and preventative strategies for related diseases [29].

2. Material and methods

2.1. Model construction

To determine how the amino acids in the vicinity help ADAMTS-5 recognize the scissile bond, two peptide sequences with 30 residues were selected from the IGD of the human aggrecan core protein:

the 359–388 peptide

PDMELPLPRNITEGE^{373} — ^{374}ARGSVILTVKPIFEV

And the 405–434 peptide

IGATAFAEVENETGE^{419} — ^{420}ATRPWGFPTPGLGPA

The former contains the scissile bond E^{373} — ^{374}A, which ADAMTS-5 actually hydrolyzes in the human body; the latter contains the same E^{419} — ^{420}A bond, which ADAMTS-5 does not catalyze. The sequences were obtained from the UniProt protein database (http://www.uniprot.org/uniprot/P16112) [30], and the peptide models were constructed by homology modeling with Modeller 9.19 [31].

The crystallographic structure of the ADAMTS-5 catalytic domain, including the metal ions bounding to it, was extracted from the Protein Data Bank (PDB ID: 2RJQ) [32]. It was then com-
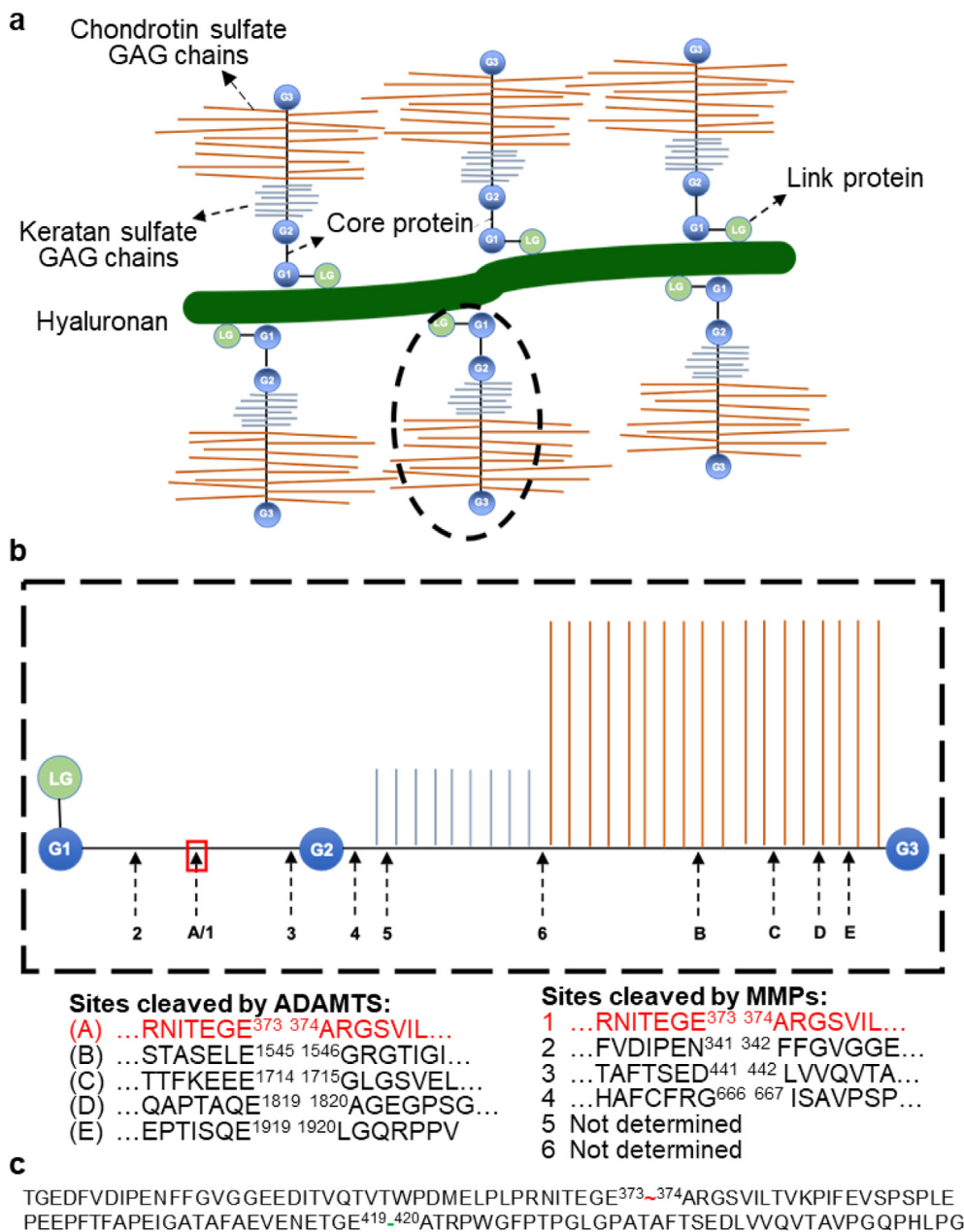
Fig. 2. Illustration of the molecular structure of aggrecan aggregates. **(a)** Aggrecan structure in the ECM. **(b)** Known cleavage sites on the aggrecan core protein. (A)–(E) represent sites cleaved by aggrecanases, and 1–6 represent those cleaved by MMPs. **(c)** Amino acid sequences in the aggrecan core protein IGD; the green dash "–" denotes the actual scissile bond, and the red tilde "~" denotes the same but noncleaved bond in the aggrecan core protein IGD. (For interpretation of the references to colour in this figure legend, the reader is referred to the web version of this article.)

bined with aggrecan peptides with Visual Molecular Dynamics (VMD) [33], constructing preliminary ADAMTS-5 complex models.

### 2.2. Molecular dynamics (MD) simulation

Molecular dynamics (MD) simulations were performed with the CHARMM27 force field [34,35] by using NAMD 2.12 [36]. Each of the ADAMTS-5 complex models was solvated in a 155 Å×126 Å×145 Å periodic water box separately. Sodium ions and chloride ions were placed in water to make the systems neutral by using the autoionize plugin of VMD, with the salt concentrations set to 0.15 mol/L. Both of the systems were energy minimized with a conjugate gradient algorithm first and then equilibrated for

80 ns in the isothermal–isobaric (NPT) ensemble at 310 K and 1 bar. The trajectories were analyzed from 50 ns to 70 ns.

2.3. Data analysis

To identify different binding poses of the aggrecan peptide, similar conformations were clustered based on the root mean square deviation (RMSD) of a specific binding site, with a cutoff of 3 Å. The RMSD of the protein backbone was calculated after aligning all frames in the trajectory to the first frame. Clustering analysis was accomplished with the Clustering Tool plugin of VMD.

The peptide binding affinity for ADAMTS-5 was analyzed in terms of both intermolecular interactions and structural fitness. Intermolecular hydrogen bonding is considered to occur when
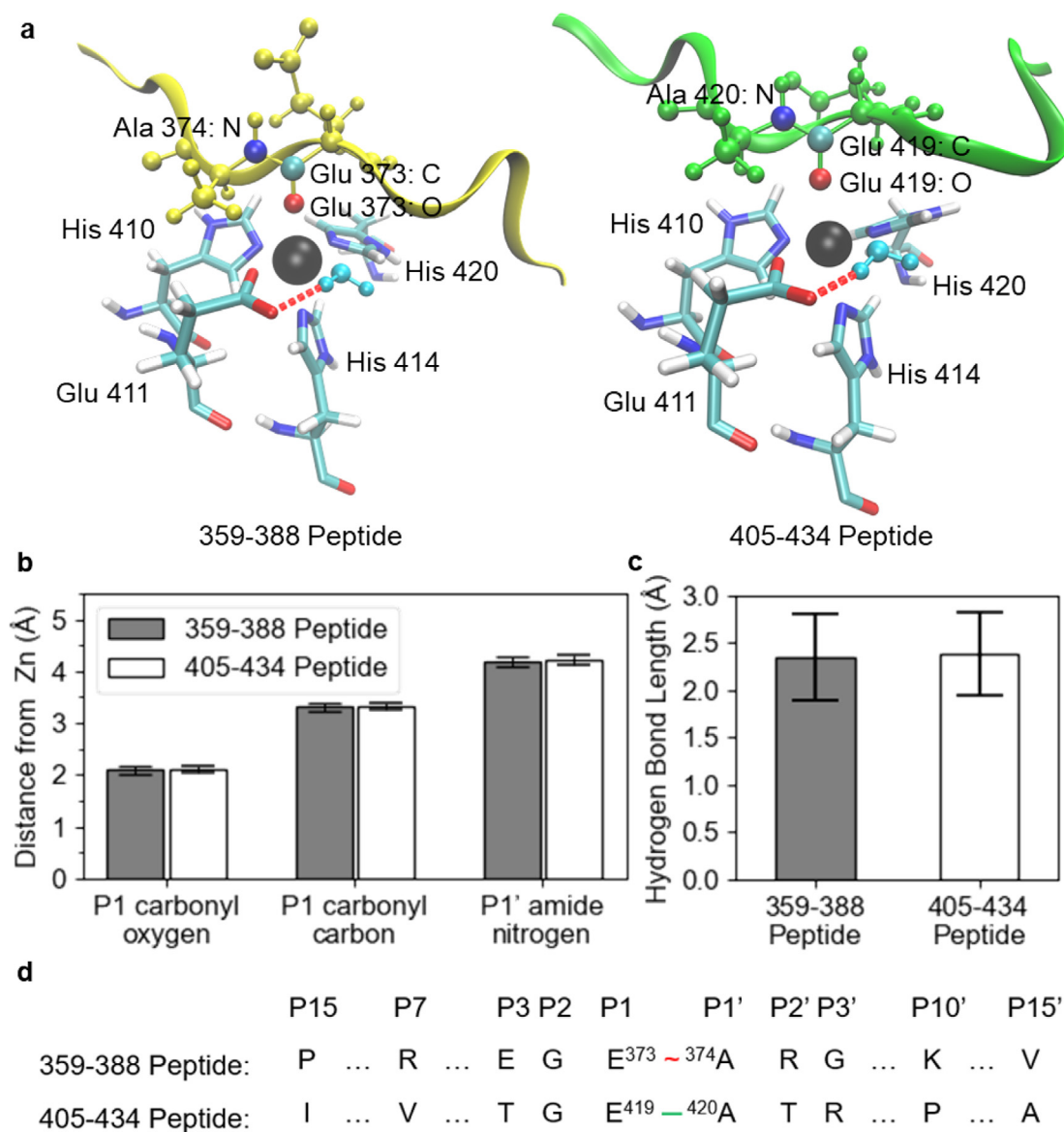
Fig. 3. Binding conformation analysis at the active site of ADAMTS-5. **(a)** Stereo view of the binding conformations of different peptides at the active site of ADAMTS-5. The zinc ions are shown as black spheres, and the zinc-bound water molecules are shown in light blue. The 359–388 peptide is shown in yellow, and the 405–434 peptide is shown in green. **(b)** Distances between the catalytic zinc ion and crucial atoms involved in the catalytic mechanism of ADAMTS-5 for different complexes. **(c)** Hydrogen bond length between zinc-bound water and Glu 411 of ADAMTS-5 for different complexes. **(d)** Amino acids at specific positions of the peptides. The green dash "–" denotes the actual scissile bond, and the red tilde "∼" denotes the same but noncleaved bond in the aggrecan core protein IGD. (For interpretation of the references to colour in this figure legend, the reader is referred to the web version of this article.)

the donor atom and the acceptor atom are within a cutoff distance of 3.5 Å and a cutoff angle of 30°. The contact frequency quantifies how well the peptides fit into ADAMTS-5, defined as the occupancy of the frames with a distance of less than 4 Å between two particular parts of the molecules in the trajectory.

The radius of gyration is used to describe the conformational differences of peptides due to their ability to fold themselves, defined as the mass-weighted root mean square distance from the molecule's center of mass [37]. To further analyze this tendency to fold, intramolecular interactions in the peptides were thus investigated, namely, intramolecular hydrogen bonds and π–π stacking interactions. Intramolecular hydrogen bonds are judged by the criteria used for intermolecular hydrogen bonds, that is, a cutoff distance of 3.5 Å and a cutoff angle of 30°. For π–π stacking interactions, the spatial relationship between two aromatic amino acids is described by their centroid–centroid separation and dihedral angle (γ). For common stacking configurations, both

slipped-parallel and T-shaped structures, the binding energy starts to decrease significantly below the Boltzmann factor as the centroid–centroid separation drops below 7.5 Å [38–40]. Hence, aromatic rings with centroid–centroid separation less than 7.5 Å are considered to have a π–π stacking interaction. To further distinguish between common π–π stacking configurations, rings with γ values from 0° to 15° are regarded as having a slipped-parallel configuration, and rings with γ values from 75° to 90° are regarded as having a T-shaped configuration.

3. Results

3.1. Binding conformations at the active site

To analyze the complexes' binding conformations at the active site, distances between critical atoms in the catalytic mechanism
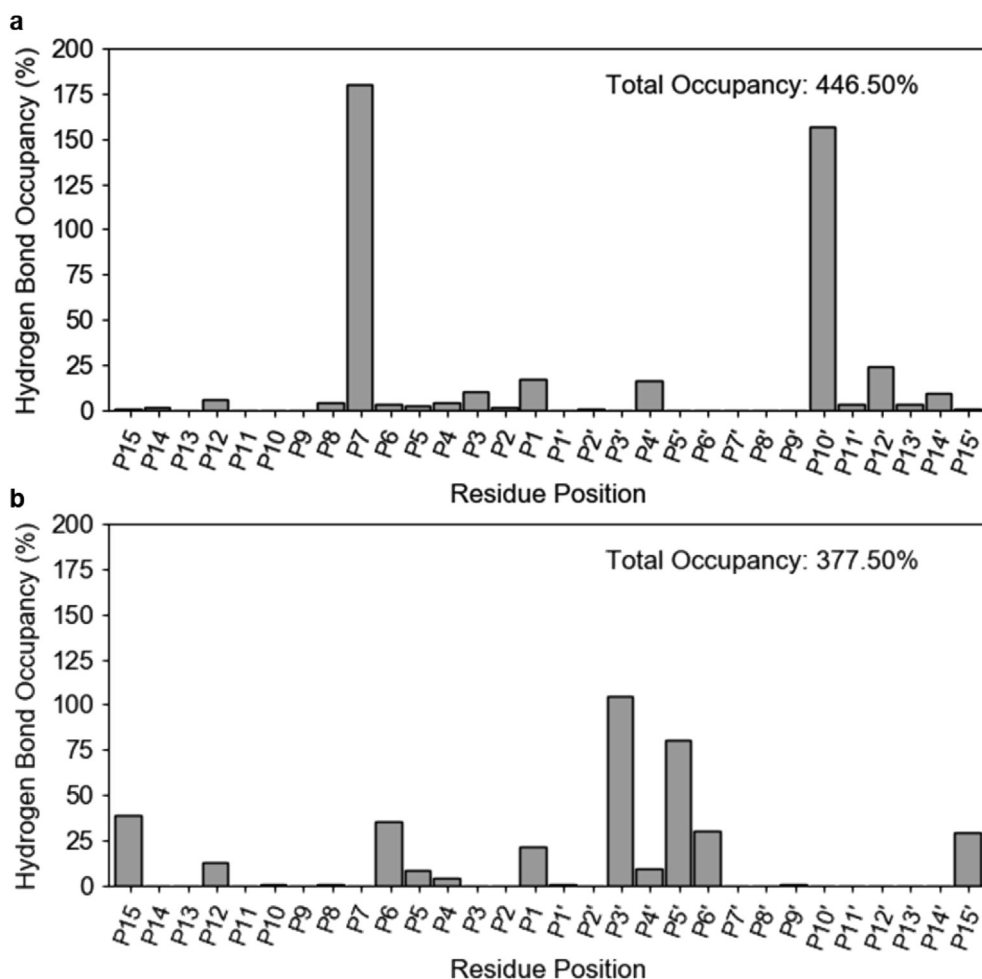
Fig. 4. Occupancy of different peptide intermolecular hydrogen bonds with ADAMTS-5. (**a**) Occupancy of hydrogen bonds between ADAMTS-5 and the 359–388 peptide. (**b**) Occupancy of hydrogen bonds between ADAMTS-5 and the 405–434 peptide. The occupancy of each residue is obtained by adding the occupancies of all hydrogen bonds to the residue formed in the trajectory.

Table 1
Hydrogen bonds between ADAMTS-5 and Arg 367 of the 359–388 peptide with occupancy higher than 10%.

Donor	Acceptor	Occupancy
Arg 367-Side-NH1	Glu 428-Side-OE2	10.50%
Arg 367-Side-NH2	Glu 428-Side-OE1	10.50%
Arg 367-Side-NH2	Glu 428-Side-OE2	10.50%
Arg 367-Side-NH1	Glu 462-Side-OE1	20.50%
Arg 367-Side-NH1	Glu 462-Side-OE2	25.50%
Arg 367-Side-NH2	Glu 462-Side-OE1	29.00%
Arg 367-Side-NH2	Glu 462-Side-OE2	20.00%

of ADAMTS-5 were calculated. The following atoms of the peptides were chosen for calculation of their distances from the catalytic zinc ion of ADAMTS-5: the P1 carbonyl oxygen, the P1 carbonyl carbon, and the P1′ amide nitrogen (Fig. 3a). The carbon atom and the nitrogen atom compose the scissile bond, and the oxygen atom is the site on the peptide that coordinates to the zinc ion [22–25]. As shown in Fig. 3b, the distances between these atoms and the zinc ion of ADAMTS-5 are very similar for both peptides. The hydrogen bond length between zinc-bound water and Glu 411 of ADAMTS-5 was also measured. In both complexes, one water molecule was found around the zinc ion. During hydrolysis, this zinc-bound water is deprotonated by Glu 411 and then attacks the carbonyl carbon of the P1 residue (Glu 373) to form a tetrahedral intermediate. Next, Glu 411 transfers the proton to the amide

nitrogen of the P1′ residue (Ala 374), finally leading to scissile bond cleavage [22–25]. As shown in Fig. 3c, the hydrogen bond length is almost the same in both complexes. The results indicate that at the active site, there is no significant structural difference in binding between the two peptides.

3.2. Intermolecular hydrogen bond number between ADAMTS-5 and the peptides

Fig. 4 shows the occupancy of hydrogen bonds between ADAMTS-5 and the peptides. The average hydrogen bond number between ADAMTS-5 and peptides was 4.5 for the 359–388 peptide (Fig. 4a) and 3.8 for the 405–434 peptide (Fig. 4b). The 359–388 peptide formed more hydrogen bonds with ADAMTS-5 on average, suggesting a more stable binding conformation. Accounting for most of the total occupancy, the occupancy of hydrogen bonds for both the P7 (Arg 367) and P10′ (Lys 383) residues in the 359–388 peptide was extremely high. The occupancy was over 150% for both residues, while in the same position of the 405–434 peptide, the P7 (Val 413) and P10′ (Pro 429) residues formed no hydrogen bonds with ADAMTS-5. This suggests that the 359–388 peptide binds to ADAMTS-5 better than the 405–434 peptide does, with P7 (Arg 367) and P10′ (Lys 383) playing an important role in this binding. The bimodal distribution of hydrogen bonds at P7 and P10′ residues provides the 359–388 peptide with more binding sites. It enables the 359–388 peptide to bind to ADAMTS-5 in a wider
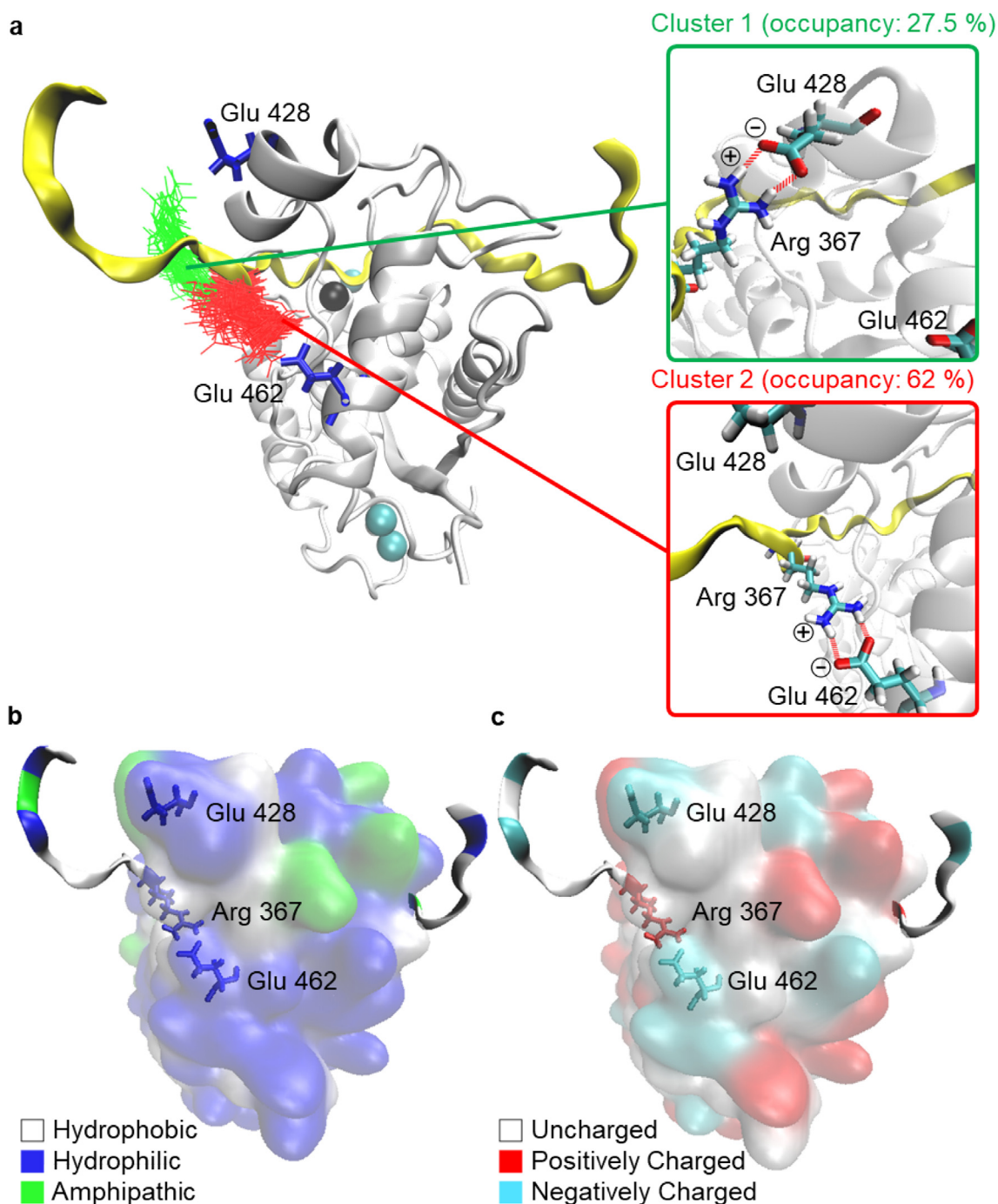
Fig. 5. Salt bridges between ADAMTS-5 and Arg 367 of the 359–388 peptide. **(a)** Two main conformations of the ADAMTS-5 complex with the 359–388 peptide, corresponding to the salt bridge Arg 367 forms. ADAMTS-5 is shown in white, and the 359–388 peptide is shown in yellow. The catalytic zinc ion is shown as a black sphere, and the calcium ions are shown as cyan spheres. **(b)** Hydrophobicity in the vicinity of the salt bridges. **(c)** Charge characteristics in the vicinity of the salt bridges. (For interpretation of the references to colour in this figure legend, the reader is referred to the web version of this article.)

range, which is instrumental in stabilizing the peptide and positioning the cleavage site. Moreover, the three-point (P7, P10′, and the cleavage site) binding mode can not only help ADAMTS-5 position the cleavage site by orienting the peptide, but also induce appropriate conformational adjustment of ADAMTS-5 that enables the peptide to fit into it better.

3.3. Binding affinity difference at position P7

In the 359–388 peptide, the hydrogen bond occupancy of the P7 residue (Arg 367) is considerably high. As shown in Table 1, Arg

367 forms hydrogen bonds with Glu 428 and Glu 462 of ADAMTS-5, which are located at its C1 and D helixes, respectively [41]. This is caused by salt bridges between the positively charged guanidinium ($RNHC(NH_2)_2^+$) of arginine and the negatively charged anionic carboxylate ($RCOO^-$) of glutamic acid. In contrast, for the 405–434 peptide, the uncharged P7 residue (Val 413) cannot form salt bridges and thus forms no hydrogen bond with ADAMTS-5.

According to the salt bridges Arg 367 forms, most of the conformations of the ADAMTS-5 complex with the 359–388 peptide were classified into two clusters (Fig. 5a). Cluster 1 is characterized by the salt bridge between Arg 367 and Glu 428, accounting for the
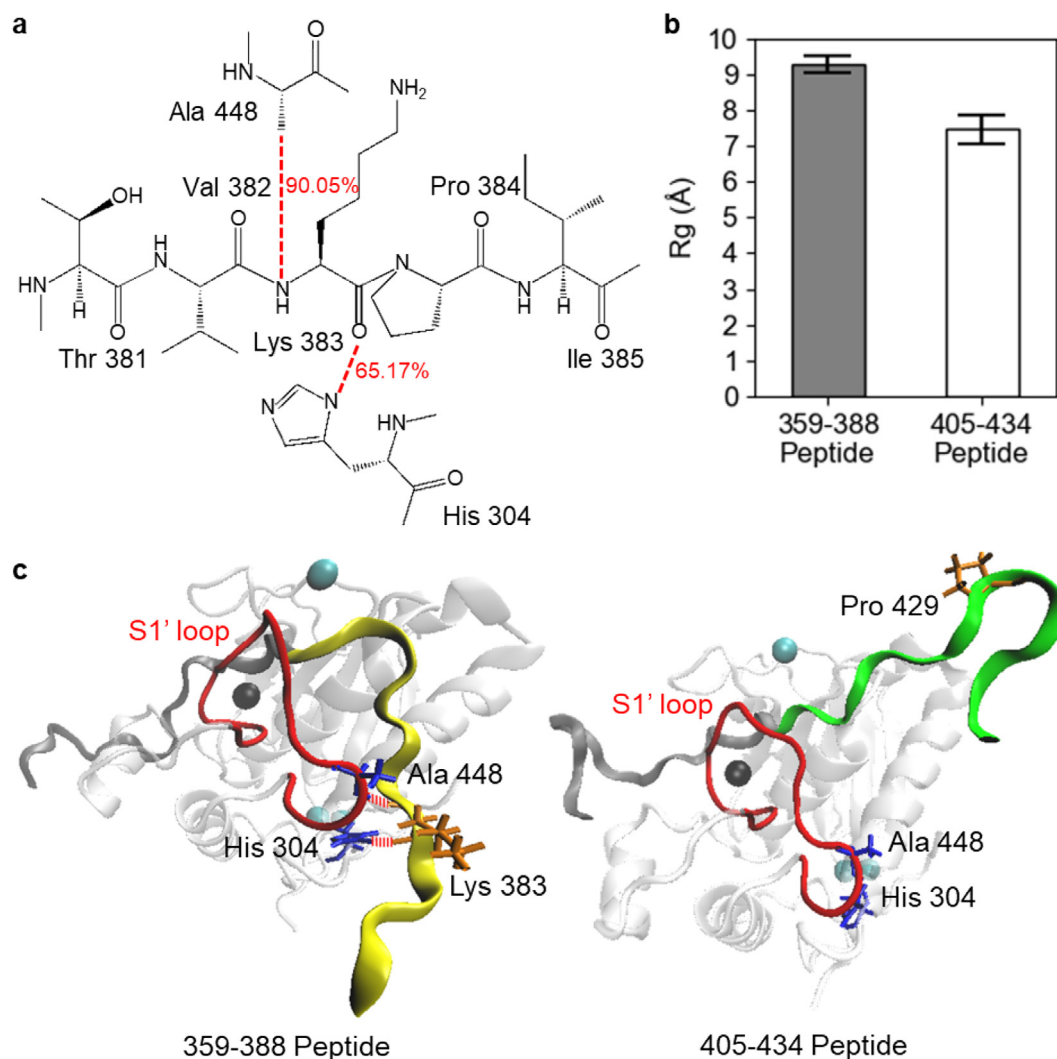
Fig. 6. Intermolecular interactions between ADAMTS-5 and the P10′ residues of different peptides. **(a)** Schematic diagram of hydrogen bonds between ADAMTS-5 and Lys 383 of the 359–388 peptide. Hydrogen bonds are represented by red dashed lines, and their occupancy is marked in red beside the lines. **(b)** Radii of gyration of the second half (P4′ to P15′ residues) of different peptides. **(c)** Stereo view of interactions between ADAMTS-5 and the second half (P4′ to P15′ residues) of different peptides. Hydrogen bonds are represented by red dashed lines. The catalytic zinc ion is shown as a black sphere, and the calcium ions are shown as cyan spheres. The second half (P4′ to P15′ residues) of the 359–388 peptide is colored yellow, and that of the 405–434 peptide is colored green. (For interpretation of the references to colour in this figure legend, the reader is referred to the web version of this article.)

first 27.5% of the trajectory, and cluster 2 is characterized by the salt bridge between Arg 367 and Glu 462, accounting for the last 62% of the trajectory. The remaining 10.5% of the conformations correspond to the transition between the two clusters. In other words, Arg 367 forms a salt bridge with Glu 428 at the beginning. Then, the salt bridge is broken, and Arg 367 forms another salt bridge with Glu 462 instead. Thus, it is inferred that Arg 367 alternately forms salt bridges with Glu 428 and Glu 462, contributing to two different binding poses of the 359–388 peptide.

Squeezed by Glu 428 and Glu 462, the 359–388 peptide swings between these residues and generates two binding poses in turn. To investigate how Arg 367 recognizes the positions of the salt bridges, the hydrophobicity and charge characteristics in the vicinity are analyzed (Fig. 5b and Fig. 5c). Arginine is positively charged and hydrophilic, and glutamic acid is negatively charged and hydrophilic. Nevertheless, the residues near the salt bridges are all uncharged and hydrophobic. Such differences in the vicinity ensure that Arg 367 attracts and forms a salt bridge with the oppositely charged Glu 428 or Glu 462 rather than other residues.

3.4. Binding affinity difference at position P10′

In addition to the P7 residue, the P10′ residue (Lys 383) in the 359–388 peptide forms hydrogen the bonds Lys 383-O⋯N-His 304 and Lys 383-N⋯O-Ala 448 with ADAMTS-5 with notably high occupancy (Fig. 6a). The binding affinity of the P10′ residue depends on the folding ability of the sequence in the vicinity, which can be measured by the peptide's radius of gyration [37]. As shown in Fig. 6b, for the second half (P4′ to P15′ residues) of the peptides, the 405–434 peptide has a lower radius of gyration than the 359–388 peptide. The former has an average radius of gyration of 7.757 Å, with a standard deviation of 0.710 Å; the latter has an average radius of gyration of 9.732 Å, with a standard deviation of 0.610 Å. That is, the second half of the 405–434 peptide tends to fold itself, making it difficult for it to bind to ADAMTS-5 well. On the other hand, with the help of the hydrogen bonds formed by Lys 383, the second half of the 359–388 peptide binds to the S1′ loop tightly (Fig. 6c).

Further insight into the peptides' folding ability can be obtained by observing their intramolecular interactions. Several intramolec-
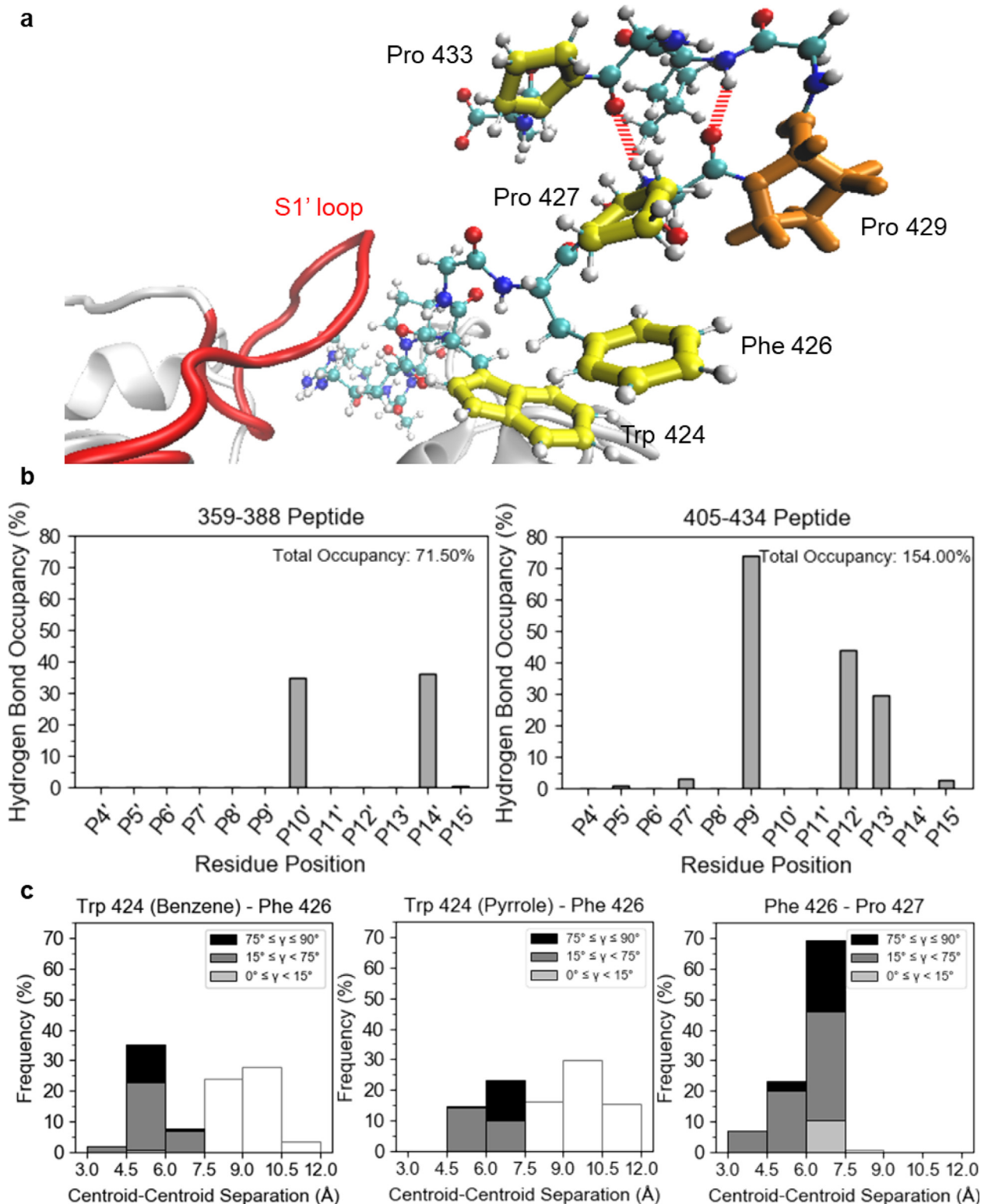
Fig. 7. Intramolecular interactions in the second half of the 405–434 peptide. **(a)** Stereo view of intramolecular interactions in the second half of the 405–434 peptide, including intramolecular hydrogen bonds and π–π stacking interactions. **(b)** Occupancy of intramolecular hydrogen bonds in the second half (P4′ to P15′ residues) of different peptides. **(c)** π–π stacking interactions in the second half (P4′ to P15′ residues) of the 405–434 peptide. In the trajectory, frames with no π–π stacking interactions (centroid–centroid separation > 7.5 Å) are marked in white. For frames with π–π stacking interactions, slipped-parallel configurations (0° < γ less than 15°) are marked in black, and T-shaped configurations (75° < γ less than 90°) are marked in light gray.

ular hydrogen bonds and π–π stacking interactions are present in the second half of the 405–434 peptide, helping it fold (Fig. 7a). For the P4′ to P15′ residues, the total occupancy of intramolecular

hydrogen bonds is 154.00% in the 405–434 peptide, while it is only 71.50% in the 359–388 peptide (Fig. 7b). In other words, intramolecular hydrogen bonds are stronger in the 405–434 pep-
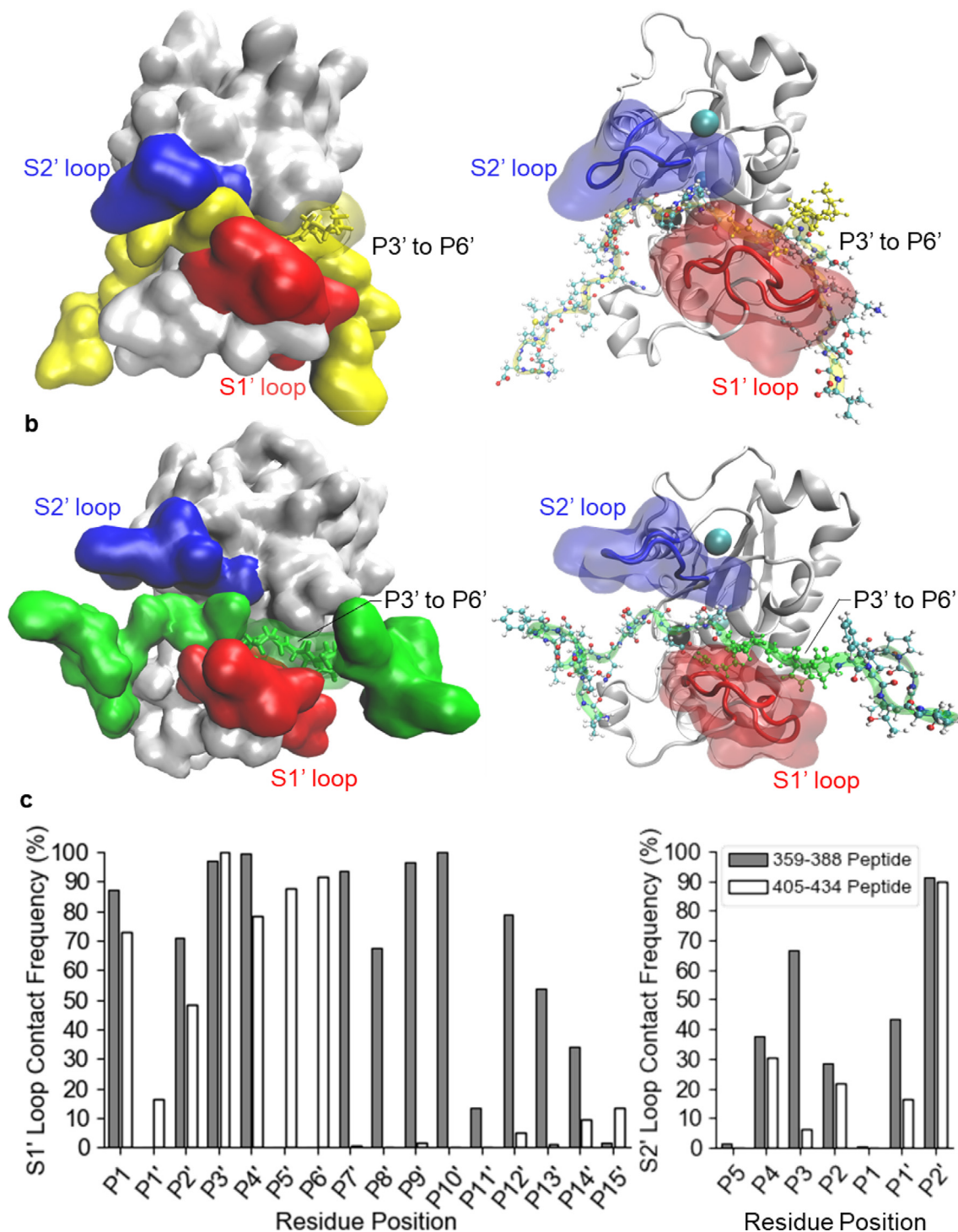
Fig. 8. Structural fitness analysis of different peptides. (**a**) Conformation of the ADAMTS-5 complex with the 359–388 peptide. (**b**) Conformation of the ADAMTS-5 complex with the 405–434 peptide. ADAMTS-5 is shown in white. The 359–388 peptide is shown in yellow, and the 405–434 peptide is shown in green. (**c**) Contact frequency with the S1′ loop and S2′ loop of ADAMTS-5 for different peptides. (For interpretation of the references to colour in this figure legend, the reader is referred to the web version of this article.)

tide. Considering that there are six aromatic residues (Pro 423, Trp 424, Phe 426, Pro 427, Pro 429, and Pro 433) in the P4′ to P15′ residues of the 405–434 peptide, π–π stacking interactions were also analyzed. Aromatic rings with centroid–centroid separation less than 7.5 Å are considered to have a π – π stacking interaction, and a dihedral angle (γ) between the ring planes is used to determine common π–π stacking configurations [38–40]. Rings with γ values from 0° to 15° are considered to have slipped-parallel con-

figurations, and rings with γ values from 75° to 90° are considered to have T-shaped configurations. Such interactions are found between aromatic residues in the P4′ to P15′ residues of the 405–434 peptide, with both T-shaped and slipped-parallel configurations appearing. In particular, among these residues, apparent π–π stacking interactions are observed in the ring pairs Trp 424-Phe 426 and Phe 426-Pro 427 (Fig. 7c). For the Trp 424-Phe 426 pair, the side-chain indole of Trp 424 consists of two rings, a six-

membered benzene and a five-membered pyrrole, both of which interact with the benzene of Phe 426. Compared with the 359–388 peptide, the 405–434 peptide contains more aromatic rings in the second half, contributing to stronger π–π stacking interactions.

3.5. Substrate stabilization enhanced by the S1′ and S2′ loops

As shown in Fig. 8a, the 359–388 peptide fits snugly into ADAMTS-5. In contrast, Fig. 8b shows that the 405–434 peptide binds to ADAMTS-5 loosely, with much space between them. The contact frequency between the 405–434 peptide and both the S1′ and S2′ loops is relatively low. The only exceptions are its P3′ to P6′ residues (Fig. 8c). Their higher contact frequency with the S1′ loop is related to their higher hydrogen bond occupancy with ADAMTS-5 in Fig. 4. The difference in the S1′ loop contact frequency between the two peptides arises from the difference in their intramolecular interactions mentioned above. The 359–388 peptide binds to the S1′ loop and wraps around it through hydrogen bonds formed by Lys 383, while the 405–434 peptide folds itself instead of attaching to the S1′ loop due to its stronger intramolecular interactions.

The flexible S1′ and S2′ loops of ADAMTS-5 are considered to be important for substrate selectivity and undergo significant conformational changes during binding [41–43]. The results indicate that the 359–388 peptide indeed fits into ADAMTS-5 better when binding. The 359–388 peptide induces a more complementary ADAMTS-5 conformation in which the S1′ and S2′ loops grab the peptide and make frequent contact with it. This suggests that the loops are responsible for not only ligand recognition but also substrate anchoring and stabilization.

4. Discussion and conclusions

This research introduces a bottom-up in silico method to elucidate the molecular mechanism by which ADAMTS-5 recognizes the exact cleavage site in the aggrecan IGD with the help of nearby sequences. In addition to the cleavage site, Arg 367 and Lys 383 also act as crucial binding sites when the 359–388 peptide binds to ADAMTS-5. In contrast, the 405–434 peptide binds to ADAMTS-5 well at only the cleavage site. Differences in the peptide sequence properties, including hydrophobicity, charge characteristics, and intramolecular interaction strength, indeed engender different binding affinities.

It is inferred that the three-point (Arg 367, Lys 383, and the cleavage site) binding mode is advantageous to the 359–388 peptide in three aspects. First, it binds more stably to ADAMTS-5. The presence of more binding sites with stronger noncovalent intermolecular interactions indicates that the peptide has higher binding affinity for ADAMTS-5. This makes ADAMTS-5 remain steadily active and able to catalyze the peptide subsequently. Second, it helps position the cleavage site. The binding sites can orient the peptide so that its cleavage site can get closer and bind to the active site of ADAMTS-5. In other words, these binding sites in the vicinity assist ADAMTS-5 in recognizing the cleavage site. Third, it induces adequate conformational changes for substrate binding. In terms of specificity, a complementary configuration is essential for enzyme catalysis. Several binding sites enable the peptide to interact with ADAMTS-5, adjusting their conformations so that the peptide fits into ADAMTS-5 better. Corresponding results were found in the structural fitness analysis, in which the 359–388 peptide fit into ADAMTS-5 more snugly, with more residues interacting with it frequently. Gripping the 359–388 peptide tightly, the peptide-induced conformations of the S1′ and S2′ loops help the enzyme stabilize and fasten the substrate.

Highlighting the importance of nearby sequences in ADAMTS-5 cleavage site recognition, this research provides insight into the mechanism of cartilage ECM degradation. It promotes medical research for related diseases such as OA, laying the cornerstone for developing regenerative medicine and preventative strategies.

Declaration of Competing Interest

The authors declare that they have no known competing financial interests or personal relationships that could have appeared to influence the work reported in this paper.

References

[1] Fosang AJ, Rogerson FM, East CJ, Stanton H. ADAMTS-5: The story so far. Eur Cells Mater 2008;15:11–26.

[2] Pratta MA, Yao W, Decicco C, Tortorella MD, Liu R-Q, Copeland RA, et al. Aggrecan protects cartilage collagen from proteolytic cleavage. J Biol Chem 2003;278(46):45539–45.

[3] Venn M, Maroudas A. Chemical composition and swelling of normal and osteoarthrotic femoral head cartilage. I. Chemical composition. Ann Rheum Dis 1977;36(2):121–9.

[4] Felisbino SL, Carvalho HF. The epiphyseal cartilage and growth of long bones in Rana catesbeiana. Tissue Cell 1999;31(3):301–7.

[5] Nap RJ, Szleifer I. Structure and Interactions of Aggrecans: Statistical Thermodynamic Approach. Biophys J 2008;95(10):4570–83.

[6] Bajpayee AG, Grodzinsky AJ. Cartilage-targeting drug delivery: can electrostatic interactions help? Nat Rev Rheumatol 2017;13:183–93.

[7] Martel-Pelletier J, Barr AJ, Cicuttini FM, Conaghan PG, Cooper C, Goldring MB, et al. Osteoarthritis. Nat Rev Dis Primers 2016;2(1). https://doi.org/10.1038/nrdp.2016.72.

[8] Hardingham TE, Fosang AJ. The structure of aggrecan and its turnover in cartilage. J Rheumatol Suppl 1995;43:86–90.

[9] KIANI C, CHEN L, WU YJ, YEE AJ, YANG BB. Structure and function of aggrecan. Cell Res 2002;12(1):19–32.

[10] Huang K, Wu LD. Aggrecanase and Aggrecan Degradation in Osteoarthritis: a Review. J Int Med Res 2008;36(6):1149–60.

[11] Buckwalter JA. The Role of Mechanical Forces in the Initiation and Progression of Osteoarthritis. HSS J 2012;8(1):37–8.

[12] Felson DT. Osteoarthritis as a disease of mechanics. Osteoarth Cartil 2013;21(1):10–5.

[13] Karamanos NK, Theocharis AD, Neill T, Iozzo RV. Matrix modeling and remodeling: A biological interplay regulating tissue homeostasis and diseases. Matrix Biol 2019;75-76:1–11.

[14] Rohani MG, Parks WC. Matrix remodeling by MMPs during wound repair. Matrix Biol 2015;44-46:113–21.

[15] Mikic B, Wong M, Chiquet M, Hunziker EB. Mechanical modulation of tenascin-C and collagen-XII expression during avian synovial joint formation. J Orthopaed Res Off Publicat Orthop Res Soc 2000;18(3):406–15.

[16] Roddy KA, Prendergast PJ, Murphy P, Agarwal S. Mechanical influences on morphogenesis of the knee joint revealed through morphological, molecular and computational analysis of immobilised embryos. PLoS ONE 2011;6(2).

[17] Nagase H, Kashiwagi M. Aggrecanases and cartilage matrix degradation. Arthritis Res Ther 2003;5:94–103.

[18] Durigova M, Nagase H, Mort JS, Roughley PJ. MMPs are less efficient than ADAMTS5 in cleaving aggrecan core protein. Matrix Biol 2011;30(2):145–53.

[19] Wang M, Shen J, Jin H, Im HJ, Sandy J, Chen D. Recent progress in understanding molecular mechanisms of cartilage degeneration during osteoarthritis. Ann N Y Acad Sci 2011;1240:61.

[20] Malemud CJ. Matrix Metalloproteinases and Synovial Joint Pathology. Prog Mol Biol Transl Sci 2017;148:305–25.

[21] Verma P, Dalal K. ADAMTS-4 and ADAMTS-5: key enzymes in osteoarthritis. J Cell Biochem 2011;112(12):3507–14.

[22] Matthews BW. Structural basis of the action of thermolysin and related zinc peptidases. Acc Chem Res 1988;21(9):333–40.

[23] Lipscomb WN, Sträter N. Recent advances in zinc enzymology. Chem Rev 1996;96(7):2375–434.

[24] McCall KA, Huang CC, Fierke CA. Function and mechanism of zinc metalloenzymes. J Nutrit 2000;130(5):1437S–46S.

[25] Miller RE, Lu Y, Tortorella MD, Malfait AM. Genetically engineered mouse models reveal the importance of proteases as osteoarthritis drug targets. Curr Rheumatol Rep 2013;15(8):350.

[26] Salsas-Escat R, Stultz CM. Conformational selection and collagenolysis in Type III collagen. Proteins 2010;78(2):325–35.

[27] Kalva S, Azhagiya Singam ER, Rajapandian V, Saleena LM, Subramanian V. Discovery of potent inhibitor for matrix metalloproteinase-9 by pharmacophore based modeling and dynamics simulation studies. J Mol Graph Model 2014;49:25–37.

[28] Patel JS, Berteotti A, Ronsisvalle S, Rocchia W, Cavalli A. Steered molecular dynamics simulations for studying protein-ligand interaction in cyclin-dependent kinase 5. J Chem Inf Model 2014;54(2):470–80.

[29] Kormi I, Nieminen MT, Havulinna AS, Zeller T, Blankenberg S, Tervahartiala T, et al. Matrix metalloproteinase-8 and tissue inhibitor of matrix metalloproteinase-1 predict incident cardiovascular disease events and all-cause mortality in a population-based cohort. Eur J Prev Cardiol 2017;24 (11):1136–44.

[30] Renaux, A. Consortium, U. UniProt: the universal protein knowledgebase (vol 45, pg D158, 2017). Nucleic Acids Res 46, 2699-2699; 2018.

[31] Fiser A, Sali A. MODELLER: Generation and refinement of homology-based protein structure models. Method Enzymol 2003;374:461–91.

[32] Mosyak L, Georgiadis K, Shane T, Svenson K, Hebert T, McDonagh T, et al. Crystal structures of the two major aggrecan degrading enzymes, ADAMTS4 and ADAMTS5. Protein Sci 2008;17(1):16–21.

[33] Humphrey W, Dalke A, Schulten K. VMD: Visual molecular dynamics. J Mol Graph Model 1996;14(1):33–8.

[34] MacKerell AD, Bashford D, Bellott M, Dunbrack RL, Evanseck JD, Field MJ, et al. All-atom empirical potential for molecular modeling and dynamics studies of proteins. J Phys Chem B 1998;102(18):3586–616.

[35] Jo S et al. CHARMM-GUI PDB manipulator for advanced modeling and simulations of proteins containing nonstandard residues. Adv Protein Chem Struct Biol 2014;96:235–65.

[36] Phillips JC, Braun R, Wang W, Gumbart J, Tajkhorshid E, Villa E, et al. Scalable molecular dynamics with NAMD. J Comput Chem 2005;26(16):1781–802.

[37] Lobanov MY, Bogatyreva NS, Galzitskaya OV. Radius of gyration as an indicator of protein structure compactness. Mol Biol 2008;42(4):623–8.

[38] McGaughey GB, Gagné M, Rappé AK. π-Stacking interactions alive and well in proteins. J Biol Chem 1998;273(25):15458–63.

[39] Yuki H, Tanaka Y, Hata M, Ishikawa H, Neya S, Hoshino T. Implementation of π-π interactions in molecular dynamics simulation. J Comput Chem 2007;28 (6):1091–9.

[40] Zhao Y, Li J, Gu H, Wei D, Xu YC, Fu W, et al. Conformational preferences of π–π stacking between ligand and protein, analysis derived from crystal structure data geometric preference of π–π interaction. Interdiscipl Sci Comput Life Sci 2015;7(3):211–20.

[41] Shieh H-S, Mathis KJ, Williams JM, Hills RL, Wiese JF, Benson TE, et al. High resolution crystal structure of the catalytic domain of ADAMTS-5 (aggrecanase-2). J Biol Chem 2008;283(3):1501–7.

[42] Filomia F, Saxena P, Durante C, de Rienzo F, Cocchi M, Menziani MC. Computational insights into ADAMTS4, ADAMTS5 and MMP13 inhibitor selectivity. Mol Inf 2012;31(6-7):421–30.

[43] Takeda S. Three-dimensional domain architecture of the ADAM family proteinases. Semin Cell Dev Biol 2009;20(2):146–52.